MIT Libraries | DSpace@MIT

MIT Open Access Articles

Lateral heterojunction photodetector consisting of molecular organic and colloidal quantum dot thin films

The MIT Faculty has made this article openly available. ***Please share*** how this access benefits you. Your story matters.

Citation: Osedach, Tim P. et al. "Lateral heterojunction photodetector consisting of molecular organic and colloidal quantum dot thin films." Applied Physics Letters 94.4 (2009): 043307-3. © 2009 American Institute of Physics

As Published: http://dx.doi.org/10.1063/1.3075577

Publisher: American Institute of Physics

Persistent URL: http://hdl.handle.net/1721.1/58589

Version: Final published version: final published article, as it appeared in a journal, conference proceedings, or other formally published context

Terms of Use: Article is made available in accordance with the publisher's policy and may be subject to US copyright law. Please refer to the publisher's site for terms of use.

Massachusetts Institute of Technology

Lateral heterojunction photodetector consisting of molecular organic and colloidal quantum dot thin films

Tim P. Osedach,[a] Scott M. Geyer, John C. Ho, Alexi C. Arango, Moungi G. Bawendi, and Vladimir Bulović[b]
Department of Electrical Engineering and Computer Science and Department of Chemistry, Massachusetts Institute of Technology, Cambridge, Massachusetts 02139, USA

(Received 1 October 2008; accepted 7 January 2009; published online 27 January 2009)

We demonstrate a heterojunction photodetector of lateral geometry that utilizes an evaporated film of the hole-transporting molecular material *N*,*N*′-bis(3-methylphenyl)-*N*,*N*′-bis(phenyl)-9,9-spirobifluorene (spiro-TPD) as a charge transport layer and that is sensitized across visible wavelengths by a thin film of colloidal CdSe nanocrystal quantum dots (QDs). High photon-to-electron quantum conversion efficiencies are obtained at room temperature as a result of photoconductive gain. With an electric field of 3.0×10^5 V/cm applied across the electrodes, we measure the external quantum efficiency at the first QD absorption peak (at wavelength $\lambda=590$ nm) to be 13%, corresponding to an internal quantum efficiency of approximately 80%. The operating mechanism of these devices is discussed, noting that the optical response is dominated by the QD absorption spectrum while the charge transport nearly exclusively takes place in the spiro-TPD. © *2009 American Institute of Physics*. [DOI: 10.1063/1.3075577]

Organic semiconductors and colloidal nanocrystal quantum dots (QDs) are promising candidate materials for realizing photovoltaics (PVs) and photodetectors (PDs) that can be fabricated near room temperature and that are scalable to large-area substrates. Organic semiconductors, including small molecules and polymers, possess a number of desirable attributes for optical sensing including high absorption coefficients over visible wavelengths and compatibility with large-area deposition processes such as ink-jet and screen printing. Various artificially nanostructured materials have also become available that possess large transition dipole moments and consequently strong optical absorption. Of particular interest among these artificial nanostructures are chemically synthesized QD nanocrystals, which, like organic semiconductors, can be processed from solution and which have a broad optical response that can be tuned from the visible to the infrared by selection of the type and physical size of the nanocrystals.[1,2]

The novelty of QD optoelectronic structures suggests the need for new device designs that optimally utilize their properties. In the present study we demonstrate a hybrid organic/QD PD in which the optical absorption and electrical charge transport are physically separated into different layers, enabling their independent tuning and optimization. This desirable capability is rare among organic photodetecting device structures with the main exception being the dye-sensitized solar cell.[3] Owing to its unique geometry, the present device also provides direct insight into the exciton dissociation mechanism that is crucial to the operation of QD PDs.

Previously, several organic PV and PD structures incorporating QDs were reported.[4–11] One class of these structures employs thin films containing QDs that are sandwiched between top and bottom contact electrodes. In the sandwich geometry, current flows vertically between the electrodes after photogenerated excitons dissociate into free carriers at a type-II heterojunction interface between the organic and QD semiconductors. Hybrid organic/QD PVs of this type have been demonstrated both in bulk heterojunction[4,5] and bilayered heterojunction[6] configurations. The second class of photosensitive structures employs thin films of organic semiconductors[7–9] or QDs (Refs. 10 and 11) that are contacted by lateral in-plane electrodes. To generate current flow in the lateral geometry voltage is applied across the electrodes facilitating extraction of the photogenerated charge.

In this letter we describe a bilayered lateral heterojunction PD comprised of a molecular thin film of *N*,*N*′-bis(3-methylphenyl) -*N*,*N*′-bis(phenyl) -9,9-spirobifluorene (spiro-TPD) and a thin film of trioctylphosphine (TOPO)-capped CdSe colloidal QDs. The device structure is shown in Fig. 1. The selection of spiro-TPD was based on its morphological stability[12] and its favorable energy band alignment with CdSe QDs.[6] The hole mobility of 10^{-4} $cm^2\ V^{-1}\ s^{-1}$ in spiro-TPD is several orders of magnitude higher than the electron mobility in the film of TOPO-capped CdSe QDs.[8,13] Therefore, in the lateral heterojunction geometry the organic layer predominantly serves as the charge transport layer. Also, because spiro-TPD does not absorb across much of the visible spectrum, it is the absorption of the QD layer that determines the long wavelength edge to the spectral sensitivity of the device.

Under illumination, excitons are generated in the organic and QD layers, which together form a type-II heterojunction (see inset of Fig. 2). Excitons within a diffusion length of this interface may be dissociated, resulting in the transfer of free electrons to the QDs and holes to the organic charge transport layer. The increase in carrier concentration results in an increase in current when a bias is applied across the electrodes.

To form the lateral PD structures, interdigitated chrome/gold electrodes (of 20 nm/50 nm film thickness, respectively)

[a]Electronic mail: osedach@mit.edu. Also at the School of Engineering and Applied Sciences, Harvard University, Cambridge, MA 02138, USA.
[b]Author to whom correspondence should be addressed. Electronic mail: bulovic@mit.edu.

 © 2009 American Institute of Physics

Downloaded 28 May 2010 to 18.51.0.132. Redistribution subject to AIP license or copyright; see http://apl.aip.org/apl/copyright.jsp

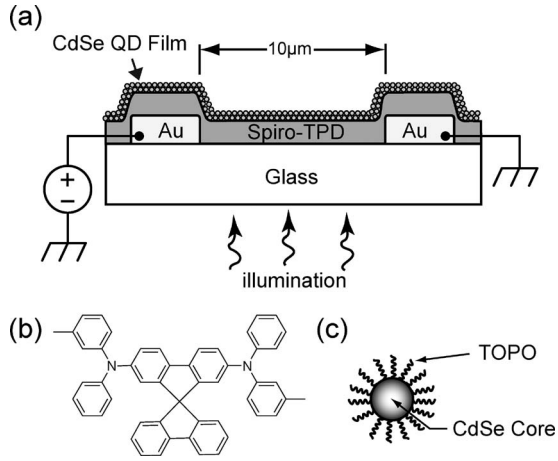

FIG. 1. (a) Section view of the device structure. The thickness of the spiro-TPD layer is 200 nm. The Au layer is 50 nm thick on top of a 20 nm thick chrome adhesion layer (not shown). For each device there are 30 pairs of Au electrodes arranged in an interdigitated array forming a serpentine channel (not shown). The channel length is 10 μm and the electrode width is 1000 μm. (b) Chemical structure of the hole-transporting material, spiro-TPD. (c) Schematic of CdSe nanocrystal passivated with TOPO ligands.

forming a serpentine channel with a length of 10 μm are first deposited by thermal evaporation onto a substrate of D263 borosilicate glass (refractive index of 1.52). A 200 nm thick spiro-TPD film (thickness measured by stylus profilometry) is then thermally evaporated over the electrodes. Subsequently, the samples are transferred directly into a nitrogen-filled glove box without exposure to air.

CdSe QD cores with a lowest energy absorption peak at wavelength $\lambda=590$ nm are synthesized and passivated by TOPO ligands to provide solubility in chloroform.[11] Microcontact printing from a polydimethylsiloxane (PDMS) stamp is used to deposit the QDs onto the device.[6,14,15] Stamps are cleaned with chloroform prior to spin-coating with QDs at 4000 rotations per minute for 60 s. The stamps coated with QDs are then placed in a vacuum environment ($\sim 10^{-3}$ Torr) for approximately 1 h to evaporate the solvent, after which a small amount of force is applied between the PDMS stamp and the device substrate to transfer the QD film. The thicknesses of transferred QD films were measured with a Digital Instruments Dimension 3000 Scanning Probe Microscope to be approximately 50 nm. Completed devices were tested immediately after fabrication at room temperature in a nitrogen environment.

Current-voltage characteristics were measured with a Keithley 6487 Picoammeter both in the dark and under illumination by a Lamina green light emitting diode (LED) light engine (emission centered at $\lambda=521$ nm) at 78 mW/cm^2. *I-V* measurements are shown in Fig. 2(a) for a control device, consisting only of the spiro-TPD film, and for a QD Device with both heterojunction layers. We note that since spiro-TPD absorption is minimal at wavelengths greater than $\lambda=400$ nm, visible light is primarily absorbed by the QDs [see Fig. 2(b)]. If we approximate the electric field distribution across the device as being constant, a bias of 100 V translates to the electric field strength of 10^5 V/cm. At this bias, the ratio of the light current to the dark current increases from 1.1, measured for the control device, to 3.5 for the QD device.

Device performance can be better understood by considering the monochromatic photon-to-electron conversion efficiency or external quantum efficiency (EQE) as a function of wavelength. For this measurement, the broadband light from a 1000 W Xe lamp was optically chopped and focused into an Acton Spectrapro 300i monochromator. A calibrated silicon PD was used to measure the optical power of the output, which was subsequently focused onto the device under study. A lock-in amplifier provided with the reference signal from the optical chopper (45 Hz) was used to extract a measurement of the ac photocurrent.

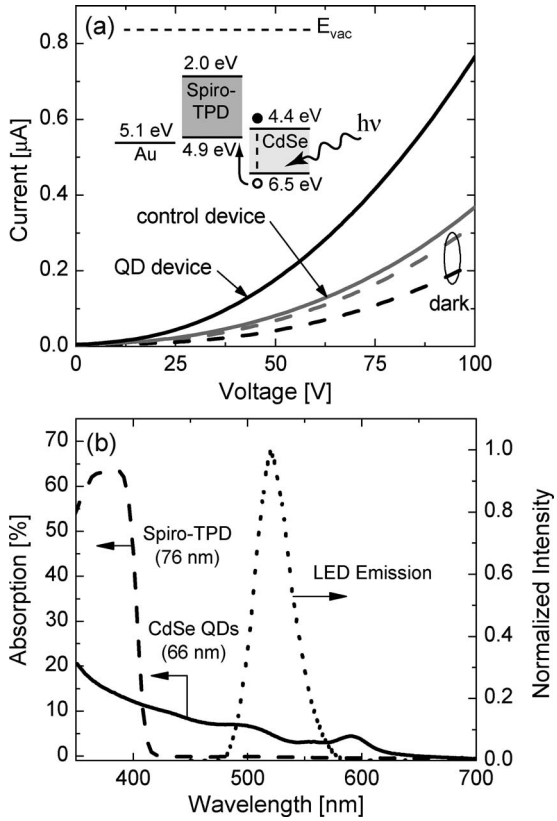

FIG. 2. (a) Current-voltage characteristics measured for a control device and a QD device. Dashed lines show dark currents. Solid lines show the device response under illumination from a green LED with an intensity of 78 mW/cm^2 and with emission centered at $\lambda=521$ nm. The inset shows the energy band diagram for the QD device. The energy levels for the spiro-TPD were taken from Ref. 12. Energy levels for the CdSe QDs were calculated following the approach reviewed in Ref. 16 and using bulk CdSe parameters obtained from Ref. 17. (b) Absorption spectra of spiro-TPD (dashed line) and CdSe QDs (solid line) measured with an Aquila NKD-8000 spectrophotometer. Emission from the LED (dotted line) is absorbed exclusively by the QD film.

Figure 3 shows the EQE of the QD device for a variety of biases. A large response peak that occurs between $\lambda=300$ nm and $\lambda=400$ nm is attributable to light that is absorbed in the spiro-TPD layer. There is also a strong photoresponse for $\lambda>400$ nm that closely follows the absorption spectrum of the QDs. A maximum in the EQE occurs at $\lambda=590$ nm, the lowest energy absorption peak of the QDs, which reaches 13% at 300 V. The EQE is related to the internal quantum efficiency (IQE) by the absorption efficiency of the device $1-T-R$, where T and R are the percentages of light that are transmitted and reflected under illumination, respectively. This relationship can be written as

$$\mathrm{EQE} = (1 - T - R) \times \mathrm{IQE}.$$

At $\lambda=590$ nm, $1-T-R$ was measured using an Aquila NKD-8000 spectrophotometer to be 16% resulting in an IQE of approximately 80%.

Downloaded 28 May 2010 to 18.51.0.132. Redistribution subject to AIP license or copyright; see http://apl.aip.org/apl/copyright.jsp

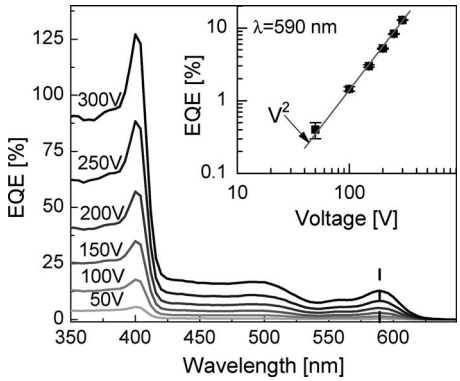

FIG. 3. EQE spectra for a variety of biases. Inset shows EQE at $\lambda=590$ nm as a function of bias. Responsivity at 400 and 590 nm are 0.41 and 0.061 A/W, respectively. Photocurrent follows a nearly V^2 power law indicative of space charge limited conduction in spiro-TPD.

For a sufficiently high bias applied across the electrodes an EQE of greater than 100% may be realized, suggesting that the device is operating in a regime of photoconductive gain. The inset reveals that the EQE measured at $\lambda=590$ nm follows a V^2 power law dependence with bias. This is consistent with space charge limited conduction in the ideal case of a trap-free low-mobility semiconductor, first described by Rose[18] and Lampert[19] and often utilized in the analysis of charge transport in organic thin films.

We note that there is a strong peak in the photoresponse at $\lambda=400$ nm, which is also where the spiro-TPD absorption begins to fall off [see Fig. 2(b)]. A photoresponse that is strongest at wavelengths for which absorption is weakest is described as antibatic. In sandwich devices, this behavior is a consequence of greater charge generation efficiency near the rear interface (the interface farthest from the source of illumination) than within the bulk. The effect is strongest if the active layer is sufficiently thick to absorb most of the incoming light.[20,21] Since the spiro-TPD film is optically thick,[22] the presence of an antibatic peak at $\lambda=400$ nm indicates that the spiro-TPD/QD interface is likely the primary site of exciton dissociation.

Finally, we note that unencapsulated devices suffered little degradation after being stored in a nitrogen environment for over 2 months. After approximately 1 week of exposure to ambient conditions, however, we observed an increase in the dark current (bias of 100 V) of greater than an order of magnitude as well as a reduction in the ratio of the light current to the dark current from 4.3 to 1.8 under identical illumination conditions.

This study demonstrates an efficient lateral PD that utilizes an evaporated film of an organic material as a charge transport layer and that is sensitized by the optical response of CdSe QDs. A type-II heterojunction at the organic/QD layer interface facilitates the dissociation of excitons and results in a large photoresponse. An antibatic peak is observed in the EQE spectrum, which suggests that exciton dissociation in the device is dominated by charge transfer at the heterointerface. Since charge generation is largely isolated to the organic/QD interface, this device structure enables the direct study of charge separation at that interface. This is in contrast to devices of the sandwich geometry, in which interfaces between active layer materials and the electrodes may complicate the interpretation of device performance.

T.P.O. was supported by a National Science Foundation Graduate Research Fellowship. S.M.G. was supported by the Martin Society of Fellows for Sustainability and the Corning Foundation. The authors would like to acknowledge stimulating and useful discussions with F. Capasso. This work was funded in part by the NSF-MRSEC Program (Grant No. DMR-0213282) through the use of its shared experimental facilities and by the U.S. Army through the Institute for Soldier Nanotechnologies under Contract No. W911NF-07-D-0004 with the U.S. Army Research Office.

[1] J. S. Steckel, S. Coe-Sullivan, V. Bulović, and M. G. Bawendi, Adv. Mater. (Weinheim, Ger.) **15**, 1862 (2003).
[2] E. H. Sargent, Adv. Mater. (Weinheim, Ger.) **17**, 515 (2005).
[3] B. O'Regan and M. Graetzel, Nature (London) **353**, 737 (1991).
[4] W. U. Huynh, J. J. Dittmer, and A. P. Alivisatos, Science **295**, 2425 (2002).
[5] D. J. Milliron, I. Gur, and A. P. Alivisatos, MRS Bull. **30**, 41 (2005).
[6] A. Arango, V. Bulović, D. C. Oertel, S. M. Geyer, and M. G. Bawendi, Nano Lett. (unpublished).
[7] T. Zukawa, S. Naka, H. Okada, and H. Onnagawa, J. Appl. Phys. **91**, 1171 (2002).
[8] T. P. I. Saragi and J. Salbeck, Appl. Phys. Lett. **89**, 253516 (2006).
[9] J. Ho, A. Arango, and V. Bulović, Appl. Phys. Lett. **93**, 063305 (2008).
[10] C. A. Leatherdale, C. R. Kagan, N. Y. Morgan, S. A. Empedocles, M. A. Kastner, and M. G. Bawendi, Phys. Rev. B **62**, 2669 (2000).
[11] M. V. Jarosz, V. J. Porter, B. R. Fisher, M. A. Kastner, and M. G. Bawendi, Phys. Rev. B **70**, 195327 (2004).
[12] T. P. I. Saragi, T. Spehr, A. Siebert, T. Fuhrmann-Lieker, and J. Salbeck, Chem. Rev. (Washington, D.C.) **107**, 1011 (2007).
[13] D. Yu, C. J. Wang, and P. Guyot-Sionnest, Science **300**, 1277 (2003).
[14] L. Kim and M. Eng, M.Eng. thesis, Massachusetts Institute of Technology, 2006.
[15] L. Kim, P. O. Anikeeva, S. A. Coe-Sullivan, J. S. Steckel, M. G. Bawendi, and V. Bulović, Nano Lett. **8**, 4513 (2008).
[16] A. L. Efros and M. Rosen, Annu. Rev. Mater. Sci. **30**, 475 (2000).
[17] T. C. Chiang and F. J. Himpsel, *Electronic Structure of Solids-Photoemission Spectra and Related Data*, Landolt-Börnstein, New Series, Group III (Springer, Berlin, 1989), Vol. 23.
[18] A. Rose, Phys. Rev. **97**, 1538 (1955).
[19] M. A. Lampert, Phys. Rev. **103**, 1648 (1956).
[20] A. K. Ghosh and T. Feng, J. Appl. Phys. **49**, 5982 (1978).
[21] N. Karl, A. Bauer, J. Holzäpfel, J. Marktanner, M. Möbus, and F. Stölzle, Mol. Cryst. Liq. Cryst. **252**, 243 (1994).
[22] The spiro-TPD film thickness is 3.2 times greater than $1/\alpha$, where α is the absorption coefficient measured to be 1.6×10^5 cm^{-1} at $\lambda=375$ nm.

Downloaded 28 May 2010 to 18.51.0.132. Redistribution subject to AIP license or copyright; see http://apl.aip.org/apl/copyright.jsp